ECS Transactions, 57 (1) 2115-2123 (2013)
10.1149/05701.2115ecst ©The Electrochemical Society

Factors that Influence Cation Segregation at the Surfaces of Perovskite Oxides

Wonyoung Lee and Bilge Yildiz

Laboratory for Electrochemical Interfaces, Department of Nuclear Science and Engineering, Massachusetts Institute of Technology, 77 Massachusetts Avenue, Cambridge, Massachusetts 02139, United States

As the oxygen reduction reaction (ORR) becomes more critical for development of solid oxide fuel cells (SOFCs) that operate at 500-700 °C, the correlation between the surface chemistry and electrochemical performance is important to understand and enable design of cathode materials with optimal surface chemistry. Recently we demonstrated that elastic and electrostatic interactions of the dopant with the host lattice drive dopant segregation, a detrimental process on the surface of perovskite cathodes (*1*). Motivated by those results, here we investigated the effects of A-site stoichiometry in $La_{0.8}Sr_{0.2}MnO_3$ (LSM) thin films on the surface chemistry and electrochemical activity. Angle-resolved X-ray photoelectron spectroscopy was employed to identify the surface cation content and chemical bonding states. A-site deficient LSM films showed higher chemical stability against Sr segregation and secondary phase formation upon annealing. This was correlated with a higher electrochemical activity measured by AC impedance spectroscopy. Given the insulating nature of secondary phases created on the surface upon annealing, observed higher electrochemical stability in A-site deficient LSM films can be ascribed to the suppressed surface segregation and phase separation.

Introduction

Cation segregation on the perovskite oxide surface imposes the significant impacts on the reactivity and stability of solid oxide fuel cell (SOFC) cathodes.(*2-9*) Oxygen reduction reaction (ORR), which is generally agreed to be limited by the surface exchange reactions on mixed ionic electronic conducting cathodes, becomes more critical for development of SOFCs that operate at 500-700 °C.(*10-12*) To attain highly reactive and stable cathode surfaces for fast ORR kinetics, it is important to understand the physical origin of cation segregation and its impacts on the electrochemical activity and stability for efficient and durable operation of SOFCs at intermediate temperatures.

Cation segregation on the perovskite oxide surfaces has been a commonly observed phenomenon, which directly impacts the surface structure and chemistry, and hence cathode reactivity and stability.(*8, 13-15*) Upon dopant segregation, the surface transforms to different chemical phases, including the perovskite-termination structure with the Sr replacing La on the A-site on the surface(*13, 15*) and phase separation in the form of Ruddlesden-Popper (RP) phases(*14*) or dopant-enriched oxides.(*2, 8, 16*)

Secondary phases on the surface can form a spatially heterogeneous surface chemistry and structure, as found on LSM,(*1*) LSC(*2*), and on STO.(*17*) Each surface structure formed upon cation segregation is associated with different ORR reactivity. A unified theory that explains the physical origins of dopant segregation on perovskite oxide surfaces and its impact on the chemical and electrochemical reactivity and stability is therefore needed for designing cathode materials with optimal surface chemistry for fast and stable ORR kinetics.

Thermodynamic and kinetic conditions that drive surface segregation and transitions to different surface phases/structures on perovskite oxides are scarce. In our recent work, we showed that cation segregation can be described by the elastic and electrostatic interactions of the dopant with the surrounding lattice in perovskite oxides.(*1*) The specific mechanisms include the size mismatch between the dopant and host cations and the associated elastic energy minimization by pushing the dopant to free surfaces or interfaces(*18-21*), and the charged defect interactions, such as a strong association of dopant cations with oxygen vacancies, which can drive the dopants to positively charged interfaces where oxygen vacancies are in abundance(*22*) as well as with polar surfaces. Based on this understanding, we propose that deficiency of the A-site cations on the perovskite lattice should suppress the dopant segregation on the A-site by allowing for more space in the bulk and reducing the elastic energy.

In this paper, we systematically assessed the effects of A-site stoichiometry in $La_{1-x}Sr_xMnO_3$ thin film surfaces on the chemical and electrochemical reactivity and stability upon thermal annealing. Angle-resolved X-ray photoelectron spectroscopy (AR-XPS) was used to probe the chemical content and environments on the film surfaces. Electrochemical impedance spectroscopy (EIS) was used to measure the cathode reactivity and stability, which coupled to chemical changes on the film surfaces. We show that the thermal annealing induced formation of the insulating secondary phases on the surface, which can hinder the ORR kinetics. Furthermore, A-site deficiency in the LSM films suppressed the cation segregation and thus secondary phase formation on the surface, which was correlated by the higher electrochemical stability at elevated temperatures. Our results demonstrate that the elastic energy in the system through A-site non-stoichiometry is an important factor to minimize the cation segregation, and therefore the electrochemical reactivity and stability of SOFC cathodes.

Experiments

Cathode Powder Preparation

Two LSM powders were synthesized with different A-site content, $(La_{0.8}Sr_{0.2})_yMnO_3$ with y = 1 (LSM100) and 0.95 (LSM95) by the modified Pechini method or polymer precursor synthesis method(*23*) using $La(NO_3)_3{\cdot}6H_2O$, $Sr(NO_3)_2$, and $Mn(NO_3)_2{\cdot}4H_2O$. Precursors were dissolved at the stoichiometric ratio in distilled water with citric acid, which was used as complexation agent. Then, ethylene glycol was added and the solution was heated till self-combustion occurred. The as-synthesized powders were subsequently calcined at 1100 °C for 6 hrs in air with ramping rate of 3 °C/min. The powders were ground in an agate mortar and pestle, and were uniaxially pressed to produce 1 inch

diameter target for pulse later deposition (PLD). The target was sintered at 1300 °C for 20 hrs with ramping rate of 3 °C/min.

Film Deposition

Single crystal 8 mol% Y_2O_3-stabilized ZrO_2 (YSZ) substrates with the (100) orientation (MTI cooperation) were used for the substrate for film deposition and the electrolyte for impedance measurements. PLD was performed with KrF excimer laser at a wavelength of 248 nm, laser beam energy of 400 mJ/pulse at 10 Hz, oxygen pressure of 10 mTorr, and the target-to-substrate distance of 6 cm. To prevent the reaction between YSZ and LSM, Gd-doped ceria (GDC) was deposited first at 450 ºC with a thickness of about 10 nm. Deposition of LSM films was performed at 750 ºC with a thickness of about 100 nm. After deposition, the sample was cooled at 10 °C/min to room temperature in an oxygen pressure of 2 Torr.

Film Characterization

A Veeco/Digital Instrument Nanoscope IV was used to perform tapping mode atomic force microscopy (AFM) for characterizing the surface morphology. Angle-resolved X-ray photoelectron spectroscopy (AR-XPS) was used to identify the cation chemistries with near-surface depth resolution on thin films. The Omicron EA 125 hemispherical analyzer and Omicron DAR 400 Mg/Al dual anode nonmonochromated X-ray source were used with Mg Kα X-ray (1253.6 eV) operated at 300 W. CasaXPS 2.3.15 software was used for spectral analysis and compositional quantification. While most samples were examined in their as-annealed conditions, as-deposited samples were examined after removing carbon contamination from their surfaces prior to the analysis. This was done by heating the samples in an oxygen pressure of ~5×10^{-5} mbar at 450-500 °C for 1.5 h in the UHV chamber.(*2*) After annealing at 800 ºC for 1 hr in air, films were quenched to preserve the surface state at elevated temperature. No additional cleaning was performed to preserve the quenched surface state. Spectra were acquired with emission angles from 0 ° to 80 ° as defined relative to the surface normal. For the excitation energy of 1253.6 eV, the sampling depths of these photoelectrons at normal emission are ~6.5 nm for Sr 3d and La 4d, ~4.0 nm for Mn 2p.(*24*) At the emission angle of 80 °, the sampling depth of each element are ~20% of those at the emission angle of 0 °, making the measurements significantly more surface sensitive.

Electrochemical Impedance Test

A photolithography technique was employed to make the Pt grid on both front and backside of LSM/GDC/YSZ samples for a better electrical contact and a higher reproducibility. A dense Pt layer with a thickness of about 100 nm was deposited suing DC sputtering. AC impedance measurements were performed from 400 °C to 800 °C in air with V_{AC} = 20 mV, V_{DC} = -0.2V, and in the frequency range from 5 mHz to 65 kHz.

Results and Discussion

We report the structural changes upon annealing in air using tapping mode atomic force microscopy. Figure 1 shows the surface morphology of LSM films to compare the

effects of annealing and A-site stoichiometry. As-deposited LSM films showed a very smooth surface with an RMS roughness of <1 nm for both LSM films. Upon annealing at 800 ºC for 1 hr in air, surface particles appeared at both LSM film surfaces. Interestingly, the formation of surface particles was remarkably suppressed in LSM95 films, i.e., A-site deficient LSM films. The RMS roughness of LSM100 films increased to 4.5 nm, and surface particles were 50-300 nm in width and 5-50 nm in height. The RMS roughness of LSM95 films increased to 1.4 nm, and surface particles were 10-50 nm in width and 2-10 nm in height. Recently we reported that one of the major driving forces for cation rearrangement is the elastic energy minimization in the system.(*1*) The LSM95, an A-site deficient film, can accommodate more of the larger cation, Sr, in the bulk lattice compared to LSM100, a stoichiometric film. The suppressed formation of surface particles in LSM95 is thus believed to be due to the more space available in the lattice for rearranged cations upon annealing, demonstrating the higher stability of A-site deficient LSM films against formation of secondary phase at the surface.

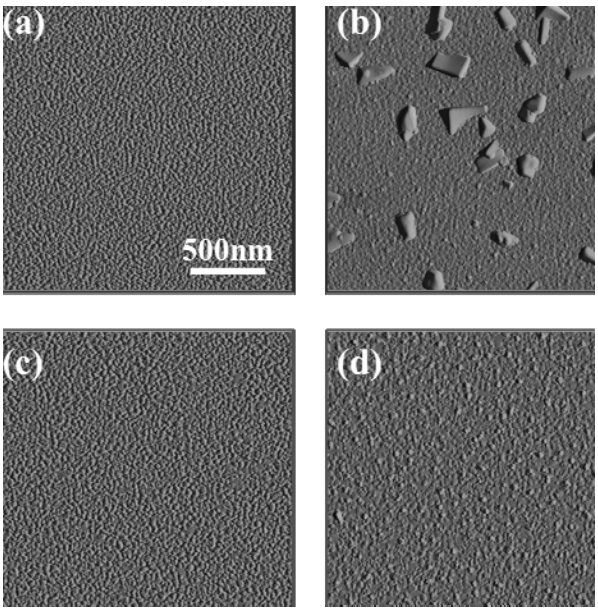

Figure 1. Surface morphologies of LSM films. (a) as-deposited LSM100 film, (b) annealed LSM100 film, (c) as-deposited LSM95 film, and (d) annealed LSM95 film. Annealing was performed at 800 °C in air for 1 hr.

To assess the impact of annealing on the surface chemistry of LSM films, angle-resolved X-ray photoelectron spectroscopy (AR-XPS) was employed with different emission angles to enable a quantitative analysis of the chemical environment as a function of depth from the film surface in a non-destructive way. (*2, 13*) High-resolution analysis of the photoemission spectra of Sr 3d core level emission was performed, at the emission angles of 0 ° and 80 ° between the sample surface normal and the detector position. The annealing-induced Sr enrichment at the surface is suppressed significantly in LSM95 compared to LSM100. Figure 2(a) shows that the increase of $Sr_{surface}/Sr_{lattice}$ ratio upon annealing was much greater in LSM100 with both emission angles. Sr/Mn ratio also increased upon annealing in both LSM samples, but much less in LSM95 with both emission angles. Similarly to structural changes upon annealing, the suppressed chemical changes at the surface were observed in A-site deficient LSM films.

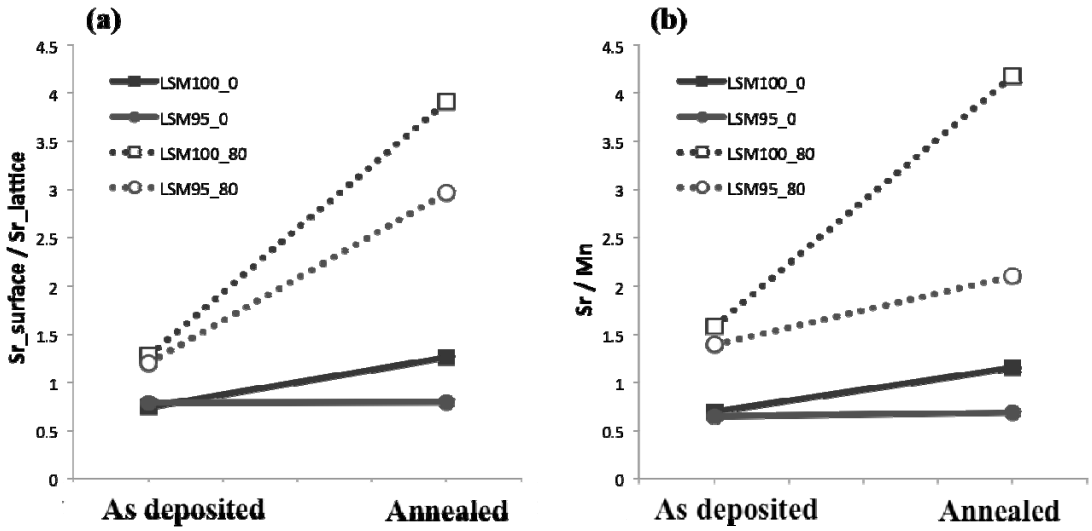

Figure 2. Cation intensity ratios of as-deposited and annealed LSM films. (a) $Sr_{surface}/Sr_{lattice}$, (b) Sr/Mn. Solid lines with closed markers and dotted lines with open markers are from the emission angle of 0 and 80, respectively. The empty and full squares and the empty and full circles are from LSM100 and LSM95, respectively.

According to structural and chemical analyses, we show that 1) Sr segregation at the very top surface even in the as-deposited films, 2) annealing promotes Sr segregation toward the surface, and 3) the A-site deficiency suppresses Sr segregation. We hypothesized that enrichment of the dopant on the A-site sublattice at the surface would lead to a larger concentration of the dopant at the surface compared to the bulk nominal level.(*1*) If the concentration of the segregated dopants increased beyond solubility limit at the perovskite surface at the elevated temperatures, phase-separated particles, such as $SrO/Sr(OH)_2$(*1, 2, 16*), or layered Ruddlesden-Popper phases(*14*) can form to minimize the elastic energy in the system. Observed substantial Sr segregation upon annealing was concurrently appeared with surface particles, suggesting that surface particles may be mainly composed of Sr, most likely Sr-oxides. Suppressed changes in the structure and chemistry in LSM95 at the surface substantiates the higher stability of A-site deficient LSM films against Sr segregation at the surface. This higher chemical stability in the A-site deficient LSM films can be ascribed to more space available for the Sr segregation in the bulk, reducing the extent of Sr enrichment at the surface.

To assess the impact of Sr segregation on the oxygen reduction activity, AC impedance spectroscopy was performed on LSM films. Figure 3 shows a representative Nyquist plot from the LSM100/GDC/YSZ sample at 700 °C in air. The total impedance is a sum of impedances at high, medium, and low frequencies. The high frequency (HF) response can be ascribed to oxygen ion transport in the electrolyte, and the medium frequency (MF) and the low frequency (LF) responses are known to originate from the chemical reactions at the electrode/electrolyte interfaces and the electrode surfaces. In our systems, the HF resistance (R_{HF}) can be mainly attributed to the ohmic resistance of the transport of O^{2-} ions through the bulk of the single crystal YSZ. The resistive component in MF (R_{MF}) is related to the transfer of O^{2-} ions across the electrode/YSZ interface.(*25*) The resistive component in LF (R_{LF}) corresponds to the dissociative adsorption and

diffusion of oxygen on the LSM surface.(*25, 26*) HF responses showed no differences among LSM films and consistent with reported literature values with an activation energy of 1.01 eV for both LSM films. Therefore, we pin down our efforts to analyze MF and LF responses, i.e., electrode impedances, in the present study.

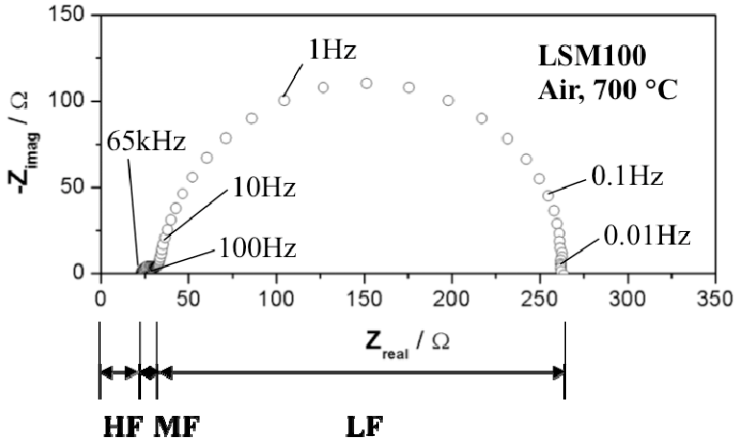

Figure 3. Nyquist plot of LSM100/GDC/YSZ sample at 700 °C in air. This impedance spectrum was obtained from the as-deposited LSM100 sample with V_{AC} = 20 mV, V_{DC} = -0.2 V, frequency = 5 mHz to 65 kHz.

Figure 6 shows the resistive components in MF and LF as a function of temperatures. To assess the evolution of electrode over the temperature, we measured the impedance twice: the first measurements while ramping up the temperature, and the second measurements while ramping down the temperature. The impedance was measured in air with the temperature range of 400-800 °C after stabilizing the temperature for 1 hr at each temperature. While increasing temperature up to 800 °C, no discernable difference in the polarization resistance, R_P (the sum of R_{MF} and R_{LF}), between LSM100 and LSM95 was observed as shown in Figure 4. While decreasing temperature from 800 °C, however, the polarization resistance, R_P showed substantial increase for both LSM films. Recall that surface structures and chemistry showed significant changes upon annealing at 800 °C: formation of surface particles, Sr-enrichment at the surface with non-perovskite phases. Severe degradation in electrode activity with changes in surface structures and chemistry was investigated in Sr-doped $LaCoO_3$ thin films and the mechanism was ascribed to formation of Sr-enriched species at the surfaces induced by the dopant segregation at elevated temperatures.(*2*) Therefore, it is reasonable to suggest that the observed degradation in electrode activity of LSM films after impedance measurements at 800 °C is induced by such changes in surface structures and chemistry. Interestingly, degradation of electrode activity depended strongly on A-site stoichiometry in LSM films. Note that LSM100 showed much higher increase in R_P compared to LSM95. R_P at 400 °C increased approximately 38.7 times and 3.7 times after impedance measurements up to 800 °C for LSM100 and LSM95, respectively, as shown in Figure 4. This means 10 times better stability for the LSM95.

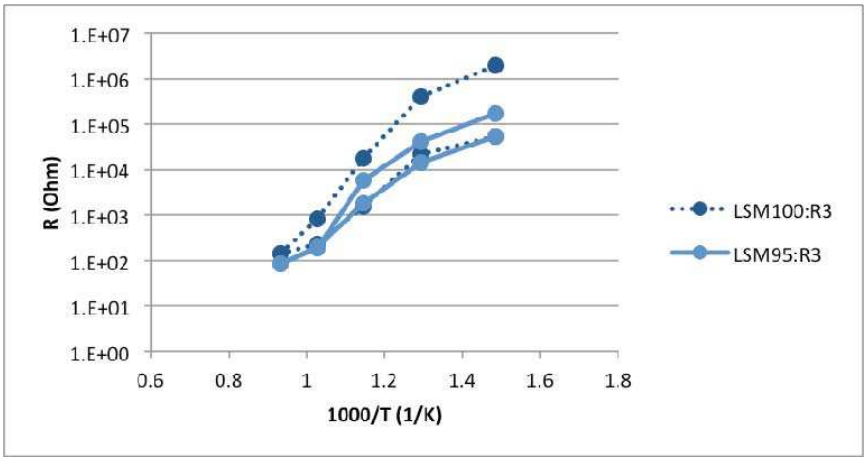

Figure 4. R_{LF} of LSM/GDC/YSZ systems with LSM95 and LSM100, measured in air as a function of temperature. The data is taken first by increasing the temperature and then decreasing the temperature, showing the degradation effect.

Direct correlation between electrode activity and surface properties substantiates that degradation of electrode activity originates from changes in surface structures and chemistry at elevated temperatures. Moreover, A-site deficiency in LSM films may alleviate Sr segregation at the surface, resulting in less change in surface structures and chemistry, and correspondingly the higher stability in electrode activity. Although both R_{MF} and R_{LF} increased significantly at elevated temperatures, R_{LF} dominated the overall performance due to its magnitude of the impedance, suggesting that R_{LF} is the rate-limiting step in cathode reactions.(*25, 26*) R_{LF} is most likely a combinational process of dissociative adsorption and diffusion limited by atomic oxygen and molecular oxygen concentration on the LSM surfaces.(*25*) Sr-enriched surface particles induced by Sr segregation at elevated temperatures may hinder oxygen reduction reactions (ORR) on the LSM surfaces due to their insulating nature. In addition, formation of Sr-enriched particles would alter the chemical stoichiometry of LSM surface, making Sr-deficient LSM films or non-stoichiometric LSM films at the surface. The partial blockage of the surface with the insulating phases and changes in stoichiometry of LSM films at the surface are found responsible for the severe electrochemical degradation of LSM film cathodes. The higher stability of LSM95, or A-site deficient LSM films, compared to LSM100 can be therefore ascribed to the lower tendency of Sr segregation toward the surface, which makes less formation of insulating phases and less change in stoichiometry in LSM films at the surface. On the other hand, R_{MF} is attributed to the migration and diffusion of oxygen species from the triple phase boundary region into the electrolyte lattices.(*25*) The presence of $La_2Zr_2O_7$ at the electrode/electrolyte interface can be reasonably excluded because of the GDC layer between the electrode and electrolyte.(*9, 27*) Changes in surface chemistry may affect the charge transfer reaction at the triple boundary region, causing degradation of ORR activity. Observed higher stability at elevated temperatures of A-site deficient LSM films demonstrates the correlation between the chemical stability and the electrode reactivity at elevated temperatures.

Conclusion

We investigated the effect of A-site stoichiometry in LSM thin films on the chemical stability and the electrode activity. Upon annealing, Sr cations were segregated on the surface, forming Sr-enriched phases. The higher stability against thermal annealing was observed from A-site deficient LSM films in terms of surface structures and chemistry, which is believed to be due to the excess space available to dopant in the A-site sublattice in the bulk. The higher polarization resistances in LSM films after measurements at 800 °C, concurrently with structural and chemical changes, show the direct correlation between the surface chemistry and the electrode activity. Furthermore, the higher stability of A-site deficient LSM films at elevated temperatures prohibits severe electrochemical degradation. These results reveal the direct correlation between the chemical stability and the electrochemical activity at high temperature, and that this relation could be tuned by controlling the A-site stoichiometry.

Acknowledgments

The authors gratefully acknowledge the financial support from the US-DOE - Office of Fossil Energy, Grant No. DE-NT0004117 for this work, and thank Caroline Ross and Harry Tuller at MIT for the use of their PLD system, and Jae Jin Kim for his help on PLD target fabrication.

References

1. W. Lee, J. W. Han, Y. Chen, Z. Cai, and B. Yildiz, *Journal of the American Chemical Society* **135**, 7909 (2013).
2. Z. Cai, M. Kubicek, J. Fleig, and B. Yildiz, *Chem. Mater.* **24**, 1116 (2012).
3. Y. Chen, W. Jung, Z. Cai, J. J. Kim, H. L. Tuller, and B. Yildiz, *Energy Environ. Sci.* **5**, 7979 (2012).
4. E. J. Crumlin, E. Mutoro, S.-J. Ahn, G. J. la O', D. N. Leonard, A. Borisevich, M. D. Biegalski, H. M. Christen, and Y. Shao-Horn, *J. Phys. Chem. Lett*. 2010, **1**(21), 3149 (2010).
5. W. Jung, H. L. Tuller, *Energy Environ. Sci.* **5**, 5370 (2012).
6. M. Kubicek, A. Limbeck, T. Frömling, H. Hutter, and J. Fleig, *J. Electrochem. Soc.* **158**, B727 (2011).
7. E. Mutoro, E. J. Crumlin, M. D. Biegalski, H. M. Christen, and Y. Shao-Horn, *Energy Environ. Sci.* **4**, 3689 (2011).
8. S. Jiang, *J. Solid State Electrochem.* **11**, 93 (2007).
9. G. J. la O, S.-J. Ahn, E. Crumlin, Y. Orikasa, M. D. Biegalski, H. M. Christen, Y. Shao-Horn, *Angewandte Chemie International Edition* **49**, 5344 (2010).
10. S. B. Adler, *Chem. Rev.* **104**, 4791 (2004).
11. Z. Shao and S. M. Haile, *Nature* **431**, 170 (2004).
12. A. Atkinson *et al.*, *Nature Materials* **3**, 17 (2004).
13. H. Jalili, J. W. Han, Y. Kuru, Z. Cai, and B. Yildiz, *J. Phys. Chem. Lett.* **2**, 801 (2011).
14. H. Dulli, P. A. Dowben, S. H. Liou, and E. W. Plummer, *Phys. Rev. B* **62**, R14629 (2000).

15. T. T. Fister, D. D. Fong, J. A. Eastman, P. M. Baldo, M. J. Highland, P. H. Fuoss, K. R. Balasubramaniam, J. C. Meador, and P. A. Salvador, *Appl. Phys. Lett.* **93**, 151904 (2008).
16. W. Wang and S. P. Jiang, *Solid State Ion.* **177**, 1361 (2006).
17. Y. Liang and D. A. Bonnell, *Surf. Sci.* **310**, 128 (1994).
18. S. Estradé, J. Arbiol, F. Peiró, Ll. Abad, V. Laukhin, Ll. Balcells and B. Martínez, *Appl. Phys. Lett.* **91**, 252503 (2007).
19. S. Estradé, J. Arbiol, F. Peiró, I. C. Infante, F. Sánchez, J. Fontcuberta, F. de la Peña, M. Walls, and C. Colliex, *Appl. Phys. Lett.* **93**, 112505 (2008).
20. S. Estradé, J. M. Rebled, J. Arbiol, F. Peiró, I. C. Infante, G. Herranz, F. Sánchez, J. Fontcuberta, R. Córdoba, B. G. Mendis, and A. L. Bleloch, *Appl. Phys. Lett.* **95**, 072507 (2009).
21. A. Lussier, J. Dvorak, S. Stadler, J. Holroyd, M. Liberati, E. Arenholz, S. B. Ogale, T. Wu, T. Venkatesan, Y.U. Idzerda, *Thin Solid Films* **516**, 880 (2008).
22. H. B. Lee, F. B. Prinz, and W. Cai, *Acta Mater.* **58**, 2197 (2010).
23. C. M. D'Souza, and N. M. Sammes, *J. Am. Ceram. Soc.* **83**, 47 (2000).
24. N. D. 82, U. S. D. o. Commerce, Ed. (Gaithersburg, MD, 2001).
25. S. P. Jiang, J. G. Love, and Y. Ramprakash, *Journal of Power Sources* **110**, 201 (2002).
26. S. P. Jiang, J. P. Zhang, and K. Foger, *Journal of The Electrochemical Society* **147**, 3195 (2000).
27. A. Chen, J. R. Smith, K. L. Duncan, R. T. DeHoff, K. S. Jones, and E. D. Wachsman, *Journal of The Electrochemical Society* **157**, B1624 (2010).